Research Article | Vol. 10, No. 10 / 1 October 2019 / Biomedical Optics Express 5136
Biomedical Optics EXPRESS

Label-free and specific detection of soluble programmed death ligand-1 using a localized surface plasmon resonance biosensor based on excessively tilted fiber gratings

BINBIN LUO,[1,3] YAJIE WANG,[1] HUAFENG LU,[1] SHENGXI WU,[2,4] YOUMING LU,[2] SHENGHUI SHI,[1] LINGCHEN LI,[2] SHANGHAI JIANG,[1] AND MINGFU ZHAO[1]

[1]*Chongqing Key Laboratory of Optical Fiber Sensor and Photoelectric Detection, Chongqing University of Technology, Chongqing 400054, China*
[2]*School of Pharmacy and Bioengineering, Chongqing University of Technology, Chongqing 400054, China*
[3]*luobinbin@cqut.edu.cn*
[4]*sxwu2004@cqut.edu.cn*

Abstract: Programmed death ligand-1 (PD-L1) plays an important role in tumor evasion from the host immune system. The level of soluble PD-L1 (sPD-L1) in serum is closely related to tumor aggressiveness and outcomes. This study aimed to propose a localized surface Plasmon resonance (LSPR) biosensor based on excessively tilted fiber grating (ExTFG) coated with large-sized (~160 nm) gold nanoshells for label-free and specific detection of sPD-L1. The experimental results showed that the limit of detection (LOD) of the immunosensor for sPD-L1 in buffer solutions was ~1 pg/mL due to the enhanced LSPR effect resulting from the interaction between sPD-L1 molecules and anti-sPD-L1 monoclonal antibodies. The detection of sPD-L1 in complex serum media, such as fetal bovine serum, confirmed that the label-free immunosensor was extremely specific to sPD-L1 and could identify it at a concentration as low as 5 pg/mL. Therefore, it can be potentially applied in clinic for the fast and early diagnosis of cancer.

1. Introduction

Cancer has become a serious threat to human life. The survival rate is still low, and, therefore, reliable biomarkers to help the early diagnosis, prevention, and treatment of cancer urgently need to be identified [1]. Nowadays, immunotherapy in cancer, namely the inhibition of the programmed death (PD)/PD-ligand 1 (PD-L1), is a very promising approach. PD-1 is an immunoglobulin superfamily type I transmembrane glycoprotein consisting of 288 amino acids. It is expressed on different immune cells, especially T cells. PD-L1 is one of the ligands of PD-1. The soluble PD-L1 (sPD-L1) is released from PD-L1-positive cells. It binds to the receptor of PD-1 and participates in immunoregulation [2,3]. PD-L1 is detected in not only lymphoid organs but also nonlymphoid tissues and is upregulated in cancer tissues. An overwhelming number of studies revealed that PD-L1 could downregulate the function of tumor-reactive cytotoxic T lymphocytes and affect survival. Blocking the interaction between PD-1 and PD-L1 using anti-PD-L1 monoclonal antibodies (anti-PD-L1 MAbs) could enhance antitumor immunity and inhibit tumor growth in vivo. Therefore, PD-L1 has been suggested to play an important role in tumor evasion from the host immune system [4]. Interestingly, recent data showed the initial sPD-L1 level was significantly associated with stage, tumor size, portal vein tumor thrombosis, and venous invasion. The overall survival was very poor in patients with a higher level of initial sPD-L1 (1.315 pg/mL). A higher level of sPD-L1 after 1 month (>12.9 pg/mL) was significantly related to early lung metastasis. In addition, a higher level of sPD-L1 might also be associated

#362729 https://doi.org/10.1364/BOE.10.005136
Journal © 2019 Received 19 Mar 2019; revised 15 Jul 2019; accepted 5 Sep 2019; published 13 Sep 2019

Biomedical Optics EXPRESS

with the prognosis of malignancies, including lung cancer [5], multiple myeloma [6], extranodal natural killer/T-cell lymphoma [7]. Patients with high serum sPD-L1 concentrations have an increased mortality risk, while very low sPD-L1 levels are associated with a better prognosis. Therefore, the level of sPD-L1 is associated with tumor aggressiveness and outcomes, suggesting its role as a possible predictive biomarker [8].

Conventionally, laboratory detection methods for sPD-L1 include immunohistochemistry (IHC) [9] enzyme-linked immunosorbent assay (ELISA) [10], and polymerase chain reaction (PCR) [11]. Currently, IHC is often performed for the qualitative analysis of the expression of sPD-L1. However, the results cannot be quantified and are of low sensitivity and specificity. ELISA is suitable for mass serological tests, but its disadvantages include time-consuming, low specificity, complex procedures, and inconvenient on-site operation. PCR possesses a high specificity by identifying the sPD-L1 gene directly, but it has been largely limited due to its high cost. Therefore, the development of a fast, accurate, and inexpensive method for immediate sPD-L1 detection has become an urgent issue for clinical researchers.

In the last decades, localized surface Plasmon resonance (LSPR) sensors have attracted great attention in biological, chemical, and environmental monitoring fields because of their high sensitivity to the surrounding refractive index (SRI) [12,13]. Unlike the surface Plasmon resonance (SPR) platform where light is radiated on the surface of a continuous metal film [14], the extinction of LSPR is caused by the absorption and scattering of light using metal nanoparticles, where the surface Plasmon polaritons are confined near the nanostructure [15]. Therefore, compared with the traditional SPR biosensors, the LSPR technology is more localized and allows for probing processes at the platform interface with spatial sensitivities well within the nanometer scale [16]. Once the biomolecules are adsorbed around the metal nanoparticles, wavelength shift and intensity variation occur in LSPR, making it extremely sensitive to the SRI changes. As gold nanoparticles are chemically inert, biologically stable, and nontoxic with high bioaffinity, many types of gold nanoparticles have been developed as supporters of LSPR, including nanospheres, nanostars, nanorods, and so on [1719]]. Moreover, various optical fiber (OF) structures are used with gold nanoparticles to produce OF-LSPR biosensors and solve the issues including huge volume and high cost of the traditional bulk prism-based SPR sensors, such as tilted fiber Bragg grating (TFBG)-based LSPR sensor [20, 21], long period fiber grating (LPFG)-based LSPR sensor [22], tapered OF-LSPR sensor [23,24], U-bent OF-LSPR probe [25], and D-shape OF-LSPR platform [26]. The aforementioned LSPR sensors focus mainly on the use of gold nanoparticles of size smaller than 100 nm, which usually have a maximal absorbance in the visible wavelength range (400–700 nm). However, among all types of gold nanoparticles, gold nanoshells are the ones that consist of an outer gold shell and an inner dielectric core with strong optical properties of absorption and scattering. Their LSPR absorption peak can be adjusted by changing the ratio of the inner and outer diameters [27,28]. Thus, their LSPR absorption band can extend to the near-infrared wavelength (up to 1600 nm) by proper design. For example, Burgmeier et al. fabricated an etched fiber Bragg grating (FBG, a diameter of ~6 μm) LSPR sensor using plasmonic gold nanoshells, which exhibited extremely high-intensity-based SRI sensitivity at ~1550 nm [29].

In this study, excessively tilted fiber gratings (ExTFGs) coupled with large-sized gold nanoshells (~160 nm) are introduced to fabricate ExTFG-LSPR sensors working at the C/L band (1525 nm~1625 nm), the SRI sensing characteristics of which have been reported in a previous study [30]. Subsequently, anti-sPD-L1 monoclonal antibodies (anti-sPD-L1 MAbs) are linked to the fabricated ExTFG-LSPR sensor surface using the staphylococcal protein A (SPA) method for the label-free and specific detection of target sPD-L1. No study has reported on the use of OF-LSPR-based biosensors for the label-free and specific detection of sPD-L1. A validation conducted in fetal bovine serum (FBS) further demonstrated the potential of the technique.

Biomedical Optics EXPRESS

2. Principle and methodology

2.1. Reagents

Analytical-grade reagents and deionized water were used for all working solutions. 3-Mercapto propyl trimethoxy silane (MPTMS) was purchased from Damas-Beta Co., Switzerland. Sodium hydroxide (NaOH, 0.2M), cysteamine, 1-ethyl-3-[3-dimethylaminopropyl] carbodiimide (EDC) hydrochloride, N-hydroxysuccinimide (NHS), and SPA (1 mg/mL) were purchased from Sigma–Aldrich, China. Phosphate-buffered solution (PBS, 0.01M, pH 7.4) and 4-morpholineethanesulfonic acid hydrate-buffered solution (MES, 0.1M, pH 6.0) were obtained from Wuhan Boster Biological Technology Co., China. The FBS (alpha-globulin, 0.7 g/dL; beta-globulin, 0.5 g/dL; endotoxin testing < 0.50 EU/mL, −20°C) sample, used as the complex buffer for the specific and clinical assessment of the functionalized ExTFG-LSPR biosensor, was purchased from Thermo Fisher Scientific, USA. Anti-sPD-L1 MAbs (150 kDa, purity more than 90%) and sPD-L1 (26 kDa, purity more than 90%) were purchased from Abcam, UK. Gold-nanoshell dispersion liquid (3.4 × 1010 particles/mL, ~160 nm) was custom-made by Beijing Deco Nanotechnology Co. Ltd, China.

The gold-nanoshell particle is composed of a solid spherical silica core wrapped with an outer gold shell. The size distribution and absorption spectrum of gold nanoshells used in this study are presented in Fig. 1(a) and (b), respectively, showing that they had a total diameter of ~160 ± 6 nm and LSPR absorption peak at ~820 nm with very broad extinction spectrum from 400 nm to 1600 nm. The gold-nanoshell dispersion was centrifuged at 10,000 rpm for 20 min to remove the sodium citrate on the particle surface before use. The LSPR absorption peak (~820 nm) of the used ~160-nm-sized gold nanoshells was closer to the C/L band compared with that (~780 nm) using relatively small (~155 nm) ones in a previous study [30]. Therefore, from this viewpoint, the size of gold nanoshells might provide an additional degree of freedom for further optimization of its LSPR absorption peak.

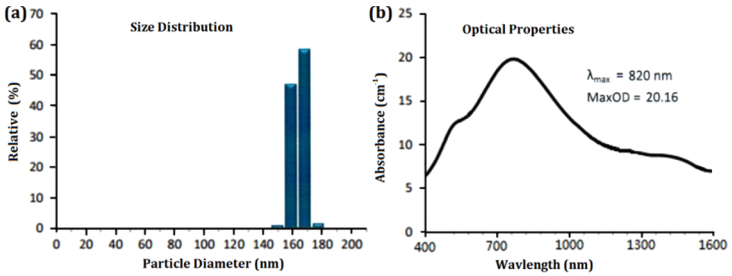

Fig. 1. (a) Size distribution, and (b) absorption spectrum of the large-sized gold nanoshells.

2.2. Fabrication of ExTFGs and apparatus

Using the scanning amplitude-mask technique and intense ultraviolet radiation with a frequency-doubled Ar+ (244 nm laser [31], several ExTFGs were inscribed in H2-loaded single-mode (SM28) fibers using identical parameters. The fabricated ExTFGs had a grating period of ~28 μm along the fiber axis, with a tilted angle of 81° and length of 8 mm. The phase-matched condition of ExTFGs was expressed as [32]:

$$\lambda_m = (n_{co}^{eff} - n_{cl,m}^{i,eff}) \cdot \frac{\Lambda_G}{\cos\theta} \qquad i = TM \text{ or } TE\,, \tag{1}$$

where λ_m^i is the resonance wavelength of transverse magnetic (TM) or transverse electric (TE) mode; n_{co}^{eff} and $n_{cl,m}^{i,eff}$ are the effective indexes of fundamental core mode and m-order cladding

Biomedical Optics EXPRESS

modes (TM or TE), respectively; Λ_G is the normal period of the grating; and θ is the tilt angle of the grating. The calibration experiments showed that the SRI sensitivity of the TM and TE modes in the C-L band of these fabricated ExTFGs was ~160 nm/RIU and ~140 nm/RIU for SRI range of 1.333~1.38, respectively. The temperature sensitivities of these ExTFGs were only ~5 pm/°C, which were far lower than that of LPFG and even lower than that of FBG, thus ensuring the stability of ExTFGs when serving as a biosensing platform.

Figure 2 shows the experimental setup for monitoring the transmission spectrum of ExTFG-LSPR sensors. The light of sweep laser source (1510nm~1590 nm, 1 Hz) from one output of the fiber optical grating demodulation system (FOGDS) (MOI-SM125, wavelength resolution 5 pm, wavelength accuracy ± 1 pm) was launched into the single-mode fiber. The isolator was used to prevent the backscattering and reflected light. The polarizer and polarization controller were used to excite and adjust the polarization statuses of the light reflected into the ExTFG-LSPR sensor. The ends of the ExTFG-LSPR sensor were fixed on two fixed glass slides, with a mobilizable glass slide between them to carry the tested liquid. The transmission spectra of the sensor were recorded using another channel of the FOGDS.

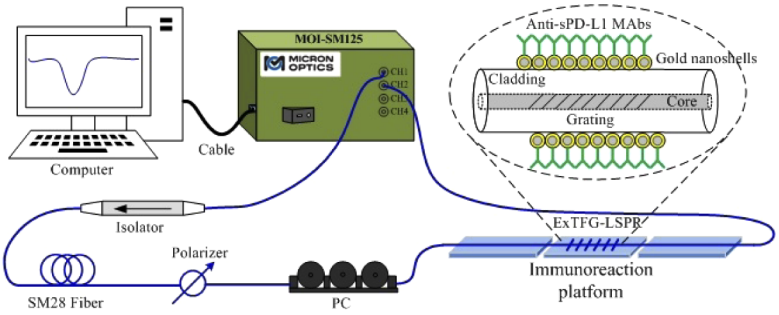

Fig. 2. Schematic diagram of the experimental setup.

2.3. Fabrication of ExTFG-LSPR sensors

The surfaces of these bare ExTFGs were cleaned using HNO_3 solution solution (5% v/v) for ~2 h at room temperature and then thoroughly washed with deionized water and ethanol. The cleaned ExTFGs were immersed in NaOH solution (0.2M) at 40°C for ~3.5 h and then at room temperature for 0.5 h to activate the hydroxyl groups (i.e., -OH) on the fiber surface. Then, the gratings were washed with deionized water several times and dried in air. Subsequently, the gratings were immediately immersed in MPTMS solution (1% v/v in glacial acetic acid) for 8 min at 65°C, and the unfixed silane compounds were thoroughly removed by washing several times with ethanol. In this salinization process, the hydrosulfonyl groups (i.e., -SH) of MPTMS were exposed on the fiber surface. Finally, the salinized ExTFGs were incubated with the prepared gold-nanoshell solution (0.2 mL) for ~12 h, allowing the gold nanoshells to link to the MPTMS layer through "Au-S" bonds (covalent bonds). Then, the gratings were washed with deionized water, thereby completing the fabrication of ExTFG-LSPR sensors.

2.4. Functionalization of ExTFG-LSPR sensors

The gold-nanoshell immobilized ExTFG-LSPR sensors were immersed in cysteamine solution (0.5mM in ultrapure water) for 1 h at room temperature. The cysteamine molecules were linked to gold nanoshells through "Au-S" bond, thus leading to the exposure of the amino groups (i.e., $-NH_2$) of cysteamine on the fiber surface. EDC (4 mg/mL in PBS, 0.01 mL) and NHS (7 mg/mL in PBS, 0.01 mL) solutions were added to the prepared SPA solution (0.5 mg/mL in MES, pH

Biomedical Optics EXPRESS

6.0, 0.18 mL) for 15 min to activate the carboxyl groups (i.e., -COOH) of SPA molecules. Next, the activated SPA solution was diluted to 0.3 mg/mL with MES, and pH was adjusted to 7.2 before use. Subsequently, the ExTFG-LSPR sensors were immersed in the activated SPA solution (0.2 mL) for 4 h at room temperature, where the carboxyl groups of SPA covalently bound to the amino groups of cysteamine, thus producing a firm SPA layer on the fiber surface. The sensors were washed with blank PBS several times. Finally, the sensors were incubated in an anti-sPD-L1-MAb solution (0.5 mg/mL in PBS, 0.2 mL) for 1 h at room temperature and then thoroughly washed with PBS to remove the unbound anti-sPD-L1-MAb molecules. The whole modified process and chemical linkage on the surface of ExTFG are depicted in Fig. 3. These fabricated ExTFG-LSPR immunosensors were covered with blank PBS (0.01M, pH 7.4) on glass slides, sealed with glass dishes, and kept at 4°C until use.

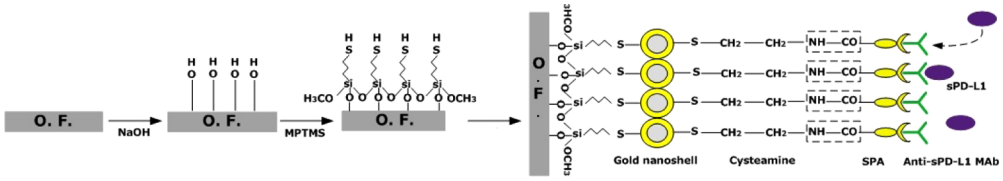

Fig. 3. Modified process and chemical linkage mechanism for ExTFG.

3. Results and discussion

3.1. Spectral properties of ExTFG-LSPR sensors

The transmission spectra of an ExTFG in water before and after gold-nanoshell immobilization were compared to investigate the spectral properties of the ExTFG-LSPR sensor. Figure 4(a) shows the spectral variation for one of the fabricated ExTFGs before and after gold-nanoshell immobilization. The resonance wavelength of the TM mode underwent a larger redshift (~3.0 nm) than that (~2.74 nm) of the TE mode due to a larger change in the effective index of the TM mode than that of the TE mode. As a consequence, the two orthogonal modes came closer after gold-nanoshell immobilization. However, the peak intensities of the TM and TE modes suffered obvious attenuation of 6.1 dBm (~66%) and 4.2 dBm (~54%), respectively, indicating effective interaction between the cladding modes of ExTFG and nanoparticles due to the wide-range LSPR absorption band of the large-sized gold nanoshells in near-infrared (NIR) range. The spectral evolutions of the ExTFG-LSPR sensor against SRI (1.333~1.38) are depicted in Fig. 4(b) and (c), exhibiting that the spectra of the TM and TE modes also suffered intensity attenuation stemming from the enhancement of LSPR effect induced by the increase in SRI. The wavelength SRI sensitivity of both the TM and TE modes increased by ~12% after the immobilization of gold nanoshells. In this study, the TM mode of ExTFG-LSPR sensors was used for biosensing experiments.

3.2. Identification of gold nanoshells immobilized on ExTFG surface

Field emission scanning electron microscope (FESEM) (Zeiss Sigma HD) images for one of the gold-nanoshell immobilized ExTFGs are shown in Fig. 5(a-d), demonstrating a large number of gold-nanoshell particles immobilized on the fiber surface. Moreover, the energy spectrum diagram and the corresponding percentage mass content of the fiber surface are shown in Fig. 5(e), indicating that Au, O, and Si elements were the main contents on the fiber surface, with “Au” and part of “O” and “Si” representing the elements of the outer gold shell and inner silica core of gold-nanoshell particles immobilized on the fiber surface. In addition, atomic force microscope (AFM, Park NX10) was used to check the surface topography of the ExTFG-LSPR sensor. As

Biomedical Optics EXPRESS

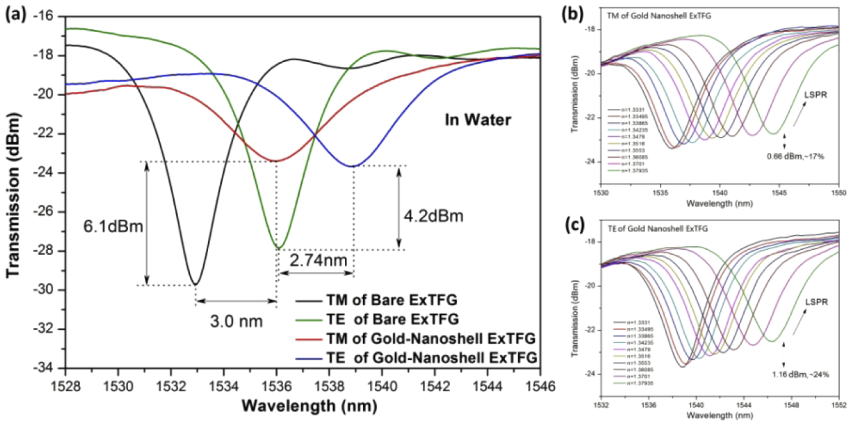

Fig. 4. Spectral change of an ExTFG in water before and after gold-nanoshell immobilization; spectral evolution versus SRI for (b) TM mode and (c) TE mode..

shown in Fig. 5(f), the surface of the sensor was very nonuniform with roughness R_a=14.917 nm. These results provided fairly good evidence for the immobilization effect of gold nanoshells on the fiber surface.

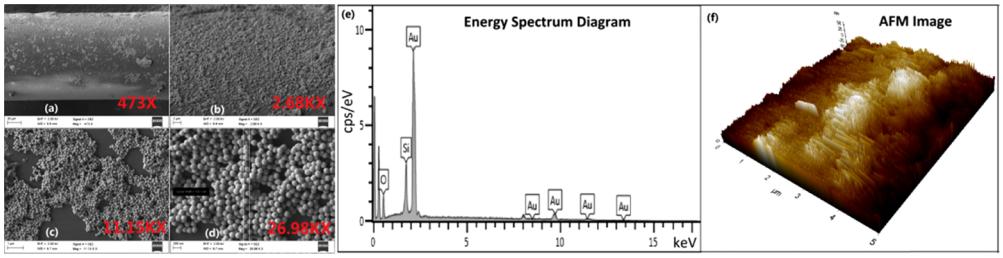

Fig. 5. FESEM images of a gold-nanoshell immobilized ExTFG (a) 473 ×, (b) 2.68 K ×, (c) 11.15 K ×, and (d) 26.98 K ×; (e) Energy spectrum diagram of an ExTFG-LSPR sensor surface; (f) AFM image of an ExTFG-LSPR sensor surface (5×5 μm).

3.3. Identification of the reactivity and specificity of anti-sPD-L1 MAbs with sPD-L1

An indirect ELISA was developed to detect the reactivity of sPD-L1with anti-sPD-L1 MAbs. In brief, 100 μL of 1 μg/mL sPD-L1 was added to the wells and incubated overnight at 4°C and washed. Anti-sPD-L1 MAbs were diluted to an appropriate dilution in PBS to be tested. Then, 100 μL of the sample was pipetted to each of the coated wells, incubated at 37°C for 1 h, and washed. Subsequently, 100 μL of the peroxidase-labeled goat anti-mouse IgG was added to the wells and incubated for 1 h at 37°C, after which the plates were washed again. Next, the substrate solution was used for the color reaction, which was stopped with the stop solution. The absorbance was immediately measured at 450 nm using an ELISA reader (Tecan Infinite 200 PRO, Switzerland). The results showed that sPD-L1 could still bind to anti-sPD-L1 MAbs when it was diluted to 7.8125 ng/mL (Fig. 6(a)). Thus, the anti-sPD-L1 MAbs possessed high activity. The specificity of anti-sPD-L1 MAbs was identified using Western blot analysis ((Fig. 6(b)). The results showed that anti-sPD-L1 MAbs reacted strongly with sPD-L1, but did not react with PD-1 control, indicating the excellent specificity of the anti-sPD-L1 MAbs.

Biomedical Optics EXPRESS

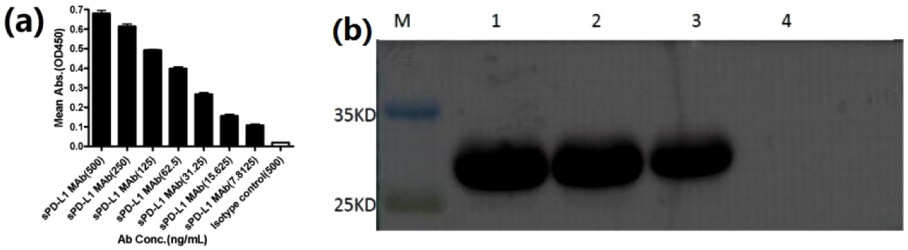

Fig. 6. (a) Reactivity of anti-sPD-L1 MAbs with sPD-L1; (b) identification of specificity of anti-sPD-L1 MAbs using Western blot analysis; lanes 1–3, sPD-L1; lane 4, PD-1 control.

3.4. Surface functionalization monitored using the spectra of ExTFGs

The whole surface modification process was also monitored using the spectra of ExTFGs. Fig.7 (a) and (b) illustrates the overall spectral evolution of one of the ExTFGs and the wavelength shifts of all ExTFGs from the beginning to the anti-sPD-L1 MAbs immobilization step, respectively. The red line (i.e., first sensor) in Fig. 7(b) represents the corresponding wavelength shifts of spectra in Fig. 7(a). Figure 7(a) indicates that the spectrum of the first ExTFG presented distinct redshifts (~3.085 nm) and intensity attenuations (~6.4 dBm) after gold-nanoshell immobilization due to the LSPR effect. The peak intensity continued to decrease after binding of SPA and anti-sPD-L1 MAbs on the fiber surface. Indeed, all other ExTFGs had similar spectral evolution behaviors as the first one. Furthermore, Fig. 7(b) shows that the relative wavelength redshifts for the SPA modified and anti-sPD-L1 MAbs immobilization steps were about 0.3~0.35 nm and 0.4~0.5 nm, respectively, due to the additional layers sticking on the fiber surface, also providing evidence for the effective surface functionalization of these sensors.

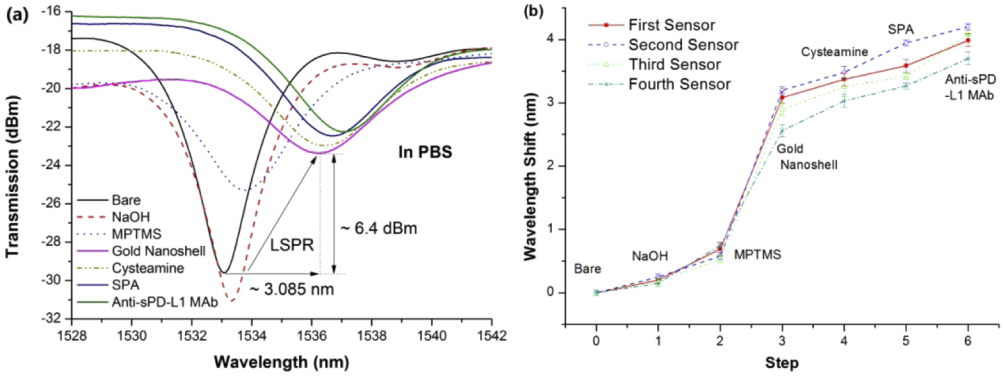

Fig. 7. (a) Spectral evolution of an ExTFG-LSPR sensor during the modified steps. (b) Corresponding wavelength shifts of all ExTFGs; the red line (first sensor) depicts the corresponding wavelength shifts of spectra in Fig. 7(a).

3.5. Detection of sPD-L1 solutions using ExTFG-LSPR immunosensors

For the first cycle of immunoassays, one of the functionalized ExTFG-LSPR immunosensors was chosen to monitor the detection performance for sPD-L1 solutions. First, a blank PBS solution was introduced to cover the grating region, and the observed resonance wavelength was recorded as the reference. Then, sPD-L1 solutions (0.2 mL) with different concentrations (1, 5, 10, 20, 50, 100, 200, 500, 1000, and 10000 pg/mL) were used for the immunoassays. The spectrum of the sensor was monitored online and recorded every 30 s until it achieved a stable status at

Biomedical Optics EXPRESS

each concentration level. Subsequently, the sensor was cleaned with blank PBS several times for the next assay of sPD-L1 solution. The aforementioned immunoassays were conducted at room temperature (25 ± 0.5°C). Since the temperature sensitivity of Ex-TFGs was extremely low (only ~5 pm/°C), the effect of temperature on the sensor response could be ignored.

Figure 8(a) and (b) shows the spectral evolution of the ExTFG-LSPR immunosensor and the corresponding resonance wavelength evolution against time during the immunoassay procedure. It also reveals that the wavelength suffered redshift of ~0.095 nm and ~0.14 nm at the concentration of 1 pg/mL and 5 pg/mL, respectively. As the wavelength resolution of the used spectral analyzer was 5 pm, the LOD of the ExTFG-LSPR immunosensor for detecting sPD-L1 was estimated to be ~1 pg/mL (i.e., 0.04pM for sPD-L1). This value was approximately 25 times lower than that obtained in a previous study using a normal-sized gold-nanosphere-integrated ExTFG sensor that had weak LSPR effects [33]. This result was reasonable because, on one hand, the absorption spectrum of large-sized gold nanoshells had an absorption peak at ~820 nm with very broad extinction spectrum from 400 nm to 1600 nm (Fig. 1(a) and (b)), ensuring that the evanescent field of the cladding mode of ExTFG at the C-L band effectively excited the LSPR of the gold nanoshells immobilized on the fiber surface. On the other hand, large-sized (~160 nm) gold nanoshells used here had a much larger specific surface area compared with that of normal size gold nanoparticles, thus increasing the sensing surface of the sensor. Moreover, because detecting small biomolecules is more challenging than detecting the large ones, it should be noted that the molecular weight of sPD-L1 (26 kDa) is much lower than that of Newcastle disease virus (NDV) (60 kDa) reported in [33]. Thus, the LOD improvement for the proposed immunosensor was considerable.

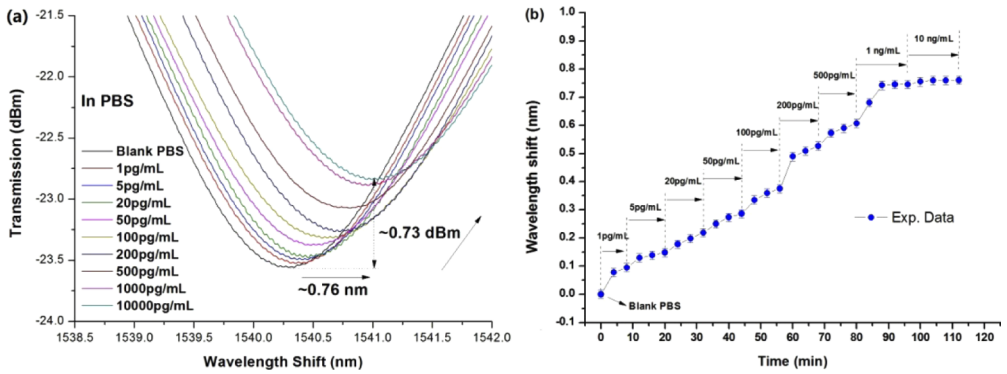

Fig. 8. (a) Spectral evolution of the first ExTFG-LSPR immunosensor for sPD-L1 detection. (b) Corresponding resonance wavelength evolution against time during the immunoassay procedure..

Figure 8 shows that the peak intensity exhibited a continuously attenuating tendency (~0.73 dBm) with the increase in the sPD-L1 concentration. This value was comparable with that (~0.66 dBm) in the SRI sensitivity calibration for the range of 1.333~1.38 (Fig. 4(b)). However, the induced SRI changes were very small for the extremely low variation of biotarget concentrations. As a consequence, the peak attenuation in Fig. 8(a) stemmed mainly from the gradually enhanced LSPR effect due to the specific interaction between targeted sPD-L1 molecules and the anti-sPD-L1 MAbs bound on gold nanoshells. From this viewpoint, the wavelength shifts of the ExTFG-LSPR sensor during the immunoassays were attributed mainly to gradually enhanced LSPR effect induced by the specific binding process of targeted sPD-L1 molecules on the fiber surface rather than the SRI change.

In addition, the wavelength showed a total redshift of ~0.75 nm at the concentration level of 1000 pg/mL and became saturated (~0.76 nm) when the concentration level was larger than 1000

Biomedical Optics EXPRESS

pg/mL, signifying that the active binding sites of anti-sPD-L1 MAbs immobilized on the fiber surface were completely occupied by the sPD-L1 antigens. Furthermore, the time response of the immunosensor in Fig. 8(b) reveals that the spectra took only approximately 5~10 min to reach a stable status at each testing concentration level, suggesting a fast detection ability of the proposed immunosensor for sPD-L1 antigens.

To verify repeatability, several other ExTFG-LSPR immunosensors were also used to conduct the aforementioned immunoassays. Fig. 9(a) shows the wavelength shifts of these immunosensors during the immunoassays; their relative standard deviation (RSD) was $0.05 < \text{RSD} < 0.07$, revealing good bio-repeatability for the devices. As shown in Figs. 5(a-d) , gold nanoshells were not ordered or configured in a monolayer architecture on the fiber surface as a consequence of the aggregation effect during the immobilization process. However, the device repeatability and bio-repeatability remained acceptable, as shown in Fig. 9. This was because the used ExTFGs were fabricated with the same parameters, simultaneously modified, and functionalized under the same circumstances with the same process. In addition, their surface topologies were basically similar, resulting in similar performances for detecting the same sPD-L1 solutions.

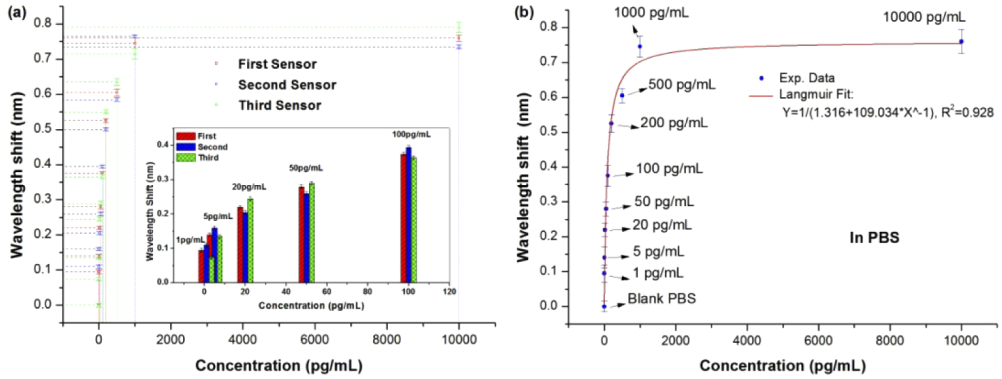

Fig. 9. (a) Wavelength shifts of immunosensors during immunoassays; their RSD was $0.05 < \text{RSD} < 0.07$ (Inset is the zoom-in image for the concentrations from 1 pg/mL to 100 pg/mL). (b) Corresponding average values of wavelength shifts and their fitting curves.

For further insight into the detection results of the ExTFG-LSPR immunosensor, Fig. 9(b) provides the corresponding average values of wavelength shifts in Fig. 9(a) as well as their fitting curves. According to the fitting results given in Fig. 9(b), the specific adsorption of the sPD-L1 molecules to the sensor surface followed the Langmuir model given by [34,35]

$$\frac{C}{\Delta\lambda} = \frac{C}{\Delta\lambda_{max}} + \frac{1}{\Delta\lambda_{max}} \cdot K_d, \tag{2}$$

where C is the concentration of sPD-L1 molecule, $\Delta\lambda$ is the wavelength shift corresponding to the sPD-L1 concentration, and $\Delta\lambda_{max}$ is the maximum value of the wavelength shift during the immunoassay process. K_d is the dissociation constant, which is an important parameter describing the binding ability between two interacting molecules to evaluate the efficiency of biosensors. The K_d between sPD-L1 and anti-sPD-L1 MAbs was determined by the least-squares fit of the data for the low sPD-L1 concentrations. The least-squares fit analysis applied to the data obtained with the proposed ExTFG-LSPR immunosensor revealed K_d to be $\sim 2.74\times10^{-12}$ M, which was comparable to that ($\sim 2.48\times10^{-12}$ M) of a similar immunosensors, for specific the detection of NDV (60 kDa) in a recent study [33]. These results indicated that the large-sized gold-nanoshell based ExTFG-LSPR sensor could be used as a biosensing platform for detecting small-scale biomolecule targets.

Biomedical Optics EXPRESS

3.6. Specific test and immunoassays in complex media

One of the functionalized ExTFG-LSPR immunosensors was used to carry out the specific tests and immunoassays in complex media, so as to check the potential clinical application. However, human serum sources are very limited. In addition, human serum use requires strict examinations and approval from the governments and organizations, such as ethics committees, with a long approval cycle. FBS has been successfully used for generating numerous human biological products due to its rich sources, convenient materials, and complete and rich nutrients, similar to human serum components (Table 1). Cytokeratin 7 peptide could be detected using FBS as a complex medium, and the desired results were obtained [36]. Therefore, in this study, the FBS concentrate was used as the complex buffer full of proteins, including albumin, IgG, enzymes, and others as well as vitamins and nutrients. The sPD-L1 sample was mixed with the FBS concentrate and PBS to prepare complex serum samples with the sPD-L1 concentrations of 5, 20, 500, and 1000 pg/mL.

Table 1. Comparison of main protein components between FBS and human serum.

	Fetal bovine serum	Human serum
Total protein content	3.5%~5.0%(w/v)	4.5%~8.5%(w/v)
Hemoglobin content	≤ 0.02% (w/v)	≤ 0.05% (w/v)

Note: Data from Chinese Pharmacopoeia.

The immunoassays were conducted by immersing the sensor in a diluted FBS solution (0.2 mL) (i.e., blank FBS) for ~20 min and then in the prepared FBS samples (0.2 mL) containing different sPD-L1 levels for ~20 min in turn. After every testing step, the sensor was thoroughly washed with PBS and then immersed in blank PBS again to record the spectrum. The spectral evolution and corresponding wavelength shifts of the sensor are shown in Fig. 10(a) and (b), respectively. It is clear that the spectrum of the ExTFG-LSPR immunosensor was nearly unchanged for blank FBS except redshifts of ~0.15 and ~0.26 nm for the FBS samples containing the sPD-L1 content of 5 pg/mL and 20 pg/mL, respectively. These redshift values were close to those (~0.14 and ~0.22 nm) measured in the PBS with identical sPD-L1 concentration levels (Fig. 9(b)). Therefore, the anti-sPD-L1-MAb-functionalized ExTFG-LSPR sensor was highly specific to sPD-L1 molecules and had high potential to be used in clinic.

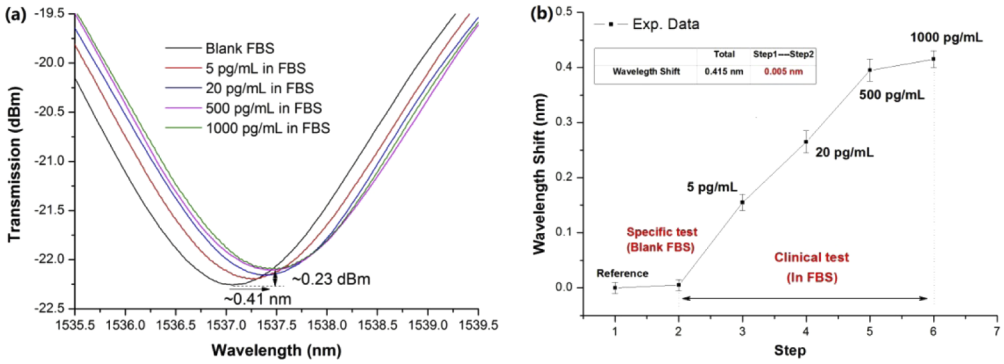

Fig. 10. (a) Spectral evolution, and (b) the corresponding wavelength shifts of the ExTFG-LSPR immunosensor for the specific test and assays in FBS samples.

Figure 10(b) shows that the response of the ExTFG-LSPR immunosensor saturated when the sPD-L1 concentration level in the FBS sample was larger than 500 pg/mL. However, the redshift (~0.4 nm) at the saturated point was only about two thirds of that (~0.6 nm) in the PBS of the

Biomedical Optics EXPRESS

identical sPD-L1 level (Fig. 9(b)). The difference in the saturation points might be because a variety of heteroproteins present in the FBS samples with the high sPD-L1 level could obviously disturb the specific binding of sPD-L1 to anti-sPD-L1 MAbs on the fiber surface.

In general, although the detection limit of the proposed immunosensors for sPD-L1 could reach ~1 pg/mL and ~5 pg/mL in PBS and FBS samples, respectively, the detection range was only 0~1 ng/mL and 0~0.5 ng/mL, respectively, which was not satisfactory. These issues could be solved using graphene oxide (GO) to encapsulate the gold nanoshells before immobilization on the fiber surface because GO possessed abundant carboxyl groups that could serve as direct antibody-binding sites. In addition, GO-encapsulated gold nanoparticles could avoid self-aggregation [37].

4. Conclusions

This study presented a large-sized gold-nanoshell (~160 nm)-immobilized ExTFG-LSPR biosensing platform. The spectral and SRI sensing characteristics of the ExTFG-LSPR sensors were demonstrated. The sensors were functionalized using anti-sPD-L1 MAbs for the label-free, fast, and specific detection of sPD-L1. The experimental results revealed that the LOD of the proposed immunosensor for target sPD-L1 molecules was ~ 1 pg/mL (i.e., 0.04pM), and the dissociation constant K_d ~2.74×10^{-12} . Furthermore, the immunoassays of sPD-L1 in FBS samples confirmed that the proposed immunosensor was extremely specific to sPD-L1 and could identify sPD-L1 at a concentration as low as 5 pg/mL. The sensitivity of the proposed ExTFG-LSPR sensors could be further improved by reducing the core/cladding diameter of ExTFGs, so as to satisfy the requirements of much lower LOD. Therefore, future studies should further optimize the proposed ExTFG-LSPR biosensors and use them to detect sPD-L1 in real human serum.

Funding

National Natural Science Foundation of China (61505017 61875026); Chongqing Science and Technology Commission (cstc2018jcyjAX0122) Natural Science Foundation of Chongqing (cstc2015jcyjBX0080); Chongqing Municipal Education Commission (KJQN201801121, KJZD-K2019011); Chongqing University of Technology (ycx2018231, ycx20192049, ycx20192068).

Acknowledgments

The authors acknowledge funding from the National Natural Science Foundation of China (61875026 and 61505017), the Foundation and cutting-edge Research Projects of Chongqing Science and Technology Commission (cstc2018jcyjAX0122), the key project of the Natural Science Foundation of Chongqing (cstc2015jcyjBX0080), The science and technology project of Chongqing Education Commission (KJQN201801121, KJZD-K2019011) and Graduate Student Innovation Program of Chongqing University of Technology (ycx2018231, ycx20192068, and ycx20192049).

Disclosures

The authors declare that there are no conflicts of interest related to this article.

References

1. S. Wu, S. Powers, W. Zhu, and Y. A. Hannun, "Substantial contribution of extrinsic risk factors to cancer development," Nature **529**(7584), 43–47 (2016).
2. Y. Chen, Q. Wang, B. Shi, P. Xu, Z. Hu, L. Bai, and X. Zhang, "Development of a sandwich ELISA for evaluating soluble PD-L1 (CD274) in human sera of different ages as well as supernatants of PD-L1+ cell lines," Cytokine+ **56**(2), 231–238 (2011).
3. K. M. Mahoney, G. J. Freeman, and D. F. McDermott, "The Next Immune-Checkpoint Inhibitors:PD-1/PD-L1 Blockade in Melanoma," Clin. Ther. **37**(4), 764–782 (2015).

Biomedical Optics EXPRESS

4. H. Dong, S. E. Strome, D. R. Salomao, H. Tamura, F. Hirano, D. B. Flies, P. C. Roche, J. Lu, G. Zhu, K. Tamada, V. A. Lennon, E. Celis, and L. Chen, "Tumor-associated B7-H1 promotes T-cell apoptosis: a potential mechanism of immune evasion," Nat. Med. **8**(8), 793–800 (2002).
5. Y. Okuma, Y. Hosomi, Y. Nakahara, K. Watanabe, Y. Sagawa, S. Homma, and J. Lung, "High plasma levels of soluble programmed cell death ligand 1 are prognostic for reduced survival in advanced lung cancer," Cancer **104**, 1–6 (2017).
6. L. Wang, H. Wang, H. Chen, W. D. Wang, X. Q. Chen, Q. R. Geng, Z. J. Xia, and Y. Lu, "Serum levels of soluble programmed death ligand 1 predict treatment response and progression free survival in multiple myeloma," Oncotarget **6**(38), 41228–41236 (2015).
7. H. Wang, L. Wang, W. J. Liu, Z. J. Xia, H. Q. Huang, W. Q. Jiang, Z. M. Li, and Y. Lu, "High post-treatment serum levels of soluble programmed cell death ligand 1 predict early relapse and poor prognosis in extranodal NK/T cell lymphoma patients," Oncotarget **7**(22), 33035–33045 (2016).
8. H. J. Kim, S. Park, K. J. Kim, and J. Seong, "Clinical significance of soluble programmed cell death ligand-1 (sPD-L1) in hepatocellular treated with radiotherapy," Radiother. Oncol. **129**(1), 130–135 (2018).
9. Q. F. Manson, N. D. Ter Hoeve, H. Buerger, C. B. Moelans, and P. J. Van Diest, "PD-1 and PD-L1 Expression in Male Breast Cancer in Comparison with Female Breast Cancer," Targ. Oncol. **13**(6), 769–777 (2018).
10. F. Finkelmeier, Ö. Canli, A. Tal, T. Pleli, J. Trojan, M. Schmidt, B. Kronenberger, S. Zeuzem, A. Piiper, F. R. Greten, and O. Waidmann, "Eur. High levels of the soluble programmed death-ligand (sPD-L1) identify hepatocellular carcinoma patients with a poor prognosis," Eur. J. Cancer **59**, 152–159 (2016).
11. D. Tan, L. Sheng, and Q. H. Yi, "Correlation of PD-1/PD-L1 polymorphisms and expressions with clinicopathologic features and prognosis of ovarian cancer," Cancer Biomarkers **21**(2), 287–297 (2018).
12. H. Taz, R. Ruther, A. Malasi, S. Yadavali, C. Carr, J. Nanda, and R. Kalyanaraman, "In situ localized surface plasmon resonance (LSPR) spectroscopy to investigate kinetics of chemical bath deposition of cds thin films," J. Phys. Chem. C **119**(9), 5033–5039 (2015).
13. L. Xie, X. Yan, and Y. Du, "An aptamer based wall-less LSPR array chip for label-free and high throughput detection of biomolecules," Biosens. Bioelectron. **53**(9), 58–64 (2014).
14. S. Patskovsky, A. V. Kabashin, M. Meunier, and J. H. Luong, "Properties and sensing characteristics of surface Plasmon resonance in infrared light," J. Opt. Soc. Am. A **20**(8), 1644–1650 (2003).
15. K. Lodewijks, R. W. Van, G. Borghs, and D. P. Van, "Boosting the figure-of-merit of LSPR-based refractive index sensing by phase-sensitive measurements," Nano Lett. **12**(3), 1655–1659 (2012).
16. S. Kaye, Z. Zeng, M. Sanders, K. Chittur, P. M. Koelle, and R. Lindquist, "Label-free detection of DNA hybridization with a compact LSPR-based fiber-optic sensor," Analyst **142**(11), 1974–1981 (2017).
17. E. Petryayeva and U. J. Krull, "Localized surface Plasmon resonance: nanostructures, bioassays and biosensing–a review," Anal. Chim. Acta **706**(1), 8–24 (2011).
18. J. Cao, M. H. Tu, T. Sun, and K. T. V. Grattan, "Wavelength-based localized surface Plasmon resonance optical fiber biosensor," Sens. Actuators, B **181**(5), 611–619 (2013).
19. M. Sanders, Y. Lin, J. Wei, T. Bono, and R. G. Lindquist, "An enhanced LSPR fiber-optic nanoprobe for ultrasensitive detection of protein biomarkers," Biosens. Bioelectron. **61**(20), 95–101 (2014).
20. S. Lepinay, A. Staff, A. Ianoul, and J. Albert, "Improved detection limits of protein optical fiber biosensors coated with gold nanoparticles," Biosens. Bioelectron. **52**(4), 337–344 (2014).
21. T. Guo, "Fiber grating-assisted surface Plasmon resonance for biochemical and electrochemical sensing," J. Lightwave Technol. **35**(16), 3323–3333 (2017).
22. J. L. Tang, S. F. Cheng, W. T. Hsu, T. Y. Chiang, and L. K. Chau, "Fiber-optic biochemical sensing with a colloidal gold-modified long period fiber grating," Sens. Actuators, B **119**(1), 105–109 (2006).
23. Q. Zhang, C. Xue, Y. Yuan, J. Lee, D. Sun, and J. Xiong, "Fiber surface modification technology for fiber-optic localized surface Plasmon resonance biosensors," Sensors **12**(3), 2729–2741 (2012).
24. S. F. Cheng and L. K. Chau, "Colloidal gold-modified optical fiber for chemical and biochemical sensing," Anal. Chem. **75**(1), 16–21 (2003).
25. D. Paul, S. Dutta, D. Saha, and R. Biswas, "LSPR based ultra-sensitive low cost U-bent optical fiber for volatile liquid sensing," Sens. Actuators, B **250**, 198–207 (2017).
26. Y. J. He, "Novel D-shape LSPR fiber sensor based on nano-metal strips," Opt. Express **21**(20), 23498–23510 (2013).
27. F. Tam, C. Moran, and N. Halas, "Geometrical parameters controlling sensitivity of nanoshell Plasmon resonances to changes in dielectric environment," J. Phys. Chem. B **108**(45), 17290–17294 (2004).
28. Y. Tao, Z. Guo, A. Zhang, J. Zhang, B. Wang, and S. Qu, "Gold nanoshells with gain-assisted silica core for ultra-sensitive bio-molecular sensors," Opt. Commun. **349**, 193–197 (2015).
29. J. Burgmeier, A. Feizpour, W. Schade, and B. M. Reinhard, "Plasmonic nanoshell functionalized etched fiber Bragg gratings for highly sensitive refractive index measurements," Opt. Lett. **40**(4), 546–549 (2015).
30. B. B. Luo, H. F. Lu, S. H. Shi, M. F. Zhao, J. Lu, Y. J. Wang, and X. Wang, "Plasmonic gold nanoshell induced spectral effects and refractive index sensing properties of excessively tilted fiber grating," Chin. Opt. Lett. **16**(10), 100603 (2018).
31. Z. Yan, H. Wang, C. L. Wang, Z. Y. Sun, G. L. Yin, K. M. Zhou, Y. S. Wang, W. Zhao, and L. Zhang, "Theoretical and experimental analysis of excessively tilted fiber gratings," Opt. Express **24**(11), 12107–12115 (2016).

Biomedical Optics EXPRESS

32. Z. Yan, Q. Sun, C. L. Wang, Z. Y. Sun, C. B. Mou, K. M. Zhou, D. Liu, and L. Zhang, "Refractive index and temperature sensitivity characterization of excessively tilted fiber grating," Opt. Express **25**(4), 3336–3346 (2017).
33. B. B. Luo, Y. F. Xu, S. X. Wu, M. F. Zhao, P. J. Jiang, S. H. Shi, Z. H. Zhang, Y. Wang, L. L. Wang, and Y. Liu, "A novel immunosensor based on excessively tilted fiber grating coated with gold nanospheres improves the detection limit of Newcastle disease virus," Biosens. Bioelectron. **100**, 169–175 (2018).
34. K. S. Chang, C. J. Sun, P. L. Chiang, A. C. Chou, M. C. Lin, and C. Liang, "Monitoring extracellular K + flux with a valinomycin-coated silicon nanowire field-effect transistor," Biosens. Bioelectron. **31**(1), 137–143 (2012).
35. B. R. Li, C. W. Chen, W. L. Yang, T. Y. Lin, C. Y. Pan, and Y. T. Chen, "Biomolecular recognition with a sensitivity-enhanced nanowire transistor biosensor," Biosens. Bioelectron. **45**(2), 252–259 (2013).
36. C. Ribaut, V. Voisin, V. Malachovská, V. Dubois, P. Mégret, R. Wattiez, and C. Caucheteur, "Small biomolecule immunosensing with plasmonic optical fiber grating sensor," Biosens. Bioelectron. **77**, 315–322 (2016).
37. J. K. Nayak, P. Parhi, and R. Jha, "Graphene oxide encapsulated gold nanoparticle based stable fibre optic sucrose sensor," Sens. Actuators, B **221**, 835–841 (2015).